AIAA JOURNAL
Vol. 45, No. 4, April 2007

# Control-Oriented Proper Orthogonal Decomposition Models for Unsteady Flows

A. Gross* and H. F. Fasel†
*University of Arizona, Tucson, Arizona 85721*

DOI: 10.2514/1.22774

**Controller development in the relatively young field of closed-loop (or feedback) flow control is constrained by the lack of proper models for the description of the dynamics and response of flows to a control input (actuation). If a set of ordinary differential equations could be derived that describes the unsteady flow with sufficient accuracy and that also models the effect of the actuation, conventional control theory tools could be employed for controller design. In this paper, reduced-order models based on a Galerkin projection of the incompressible Navier–Stokes equations onto a proper orthogonal decomposition modal basis are described. The model coefficients can be modified or calibrated to make the model more accurate. An error-minimization technique is employed to obtain the coefficients that describe how the control input enters the model equations. These models work well in the vicinity of the design operating point. Composite models are constructed by combining modes from different operating points. This approach results in more versatile models that are valid for a larger range of operating conditions.**

## Nomenclature

| | | |
|---|---|---|
| $A$ | = | modes 1 and 2 amplitudes |
| $\mathbf{a}$ | = | vector of time coefficients |
| $a_i$ | = | time coefficient |
| $\mathbf{C}$ | = | correlation tensor |
| $C_x$ | = | axial chord length |
| $c$ | = | cubic model coefficient |
| $\mathbf{E}$ | = | Jacobian of model error |
| $e$ | = | kinetic energy |
| $\mathbf{e}$ | = | model error |
| $F^+$ | = | nondimensional forcing frequency |
| $f$ | = | forcing term model coefficient |
| $\mathbf{f}, \mathbf{g}$ | = | auxiliary vectors for model calibration |
| $I$ | = | number of modes |
| $J$ | = | number of actuation modes |
| $\mathcal{J}$ | = | compound error |
| $l$ | = | linear model coefficient |
| $m_k$ | = | monomial basis |
| $N$ | = | number of time steps |
| $\mathbf{n}$ | = | boundary-normal vector |
| $p$ | = | static pressure |
| $q$ | = | quadratic model coefficient |
| $\mathbf{q}$ | = | eigenmode |
| $Re$ | = | Reynolds number |
| $\mathbf{r}$ | = | correlation tensor eigenvector |
| $T$ | = | time interval |
| $t$ | = | time |
| $\mathbf{v}$ | = | velocity field |
| $\mathbf{y}$ | = | vector of model coefficients |
| $\alpha$ | = | calibration parameter |
| $\delta_{ij}$ | = | Kronecker symbol |
| $\lambda_i$ | = | eigenvalue |
| $\nu_i$ | = | viscous parameter |
| $\varphi$ | = | modes 1 and 2 phase |

*Subscripts*

| | | |
|---|---|---|
| $i, j, k, l$ | = | mode indices |
| $\partial\Omega$ | = | domain boundary |
| $\Omega$ | = | domain, indicating inner product |

*Superscripts*

| | | |
|---|---|---|
| $e$ | = | reference, experimental |
| $g$ | = | from Galerkin projection |
| $n$ | = | time step |
| $\alpha$ | = | calibrated |

## Introduction

WHEN the geometric shape of an aerodynamic body is fixed and means for passive flow control have been fully exploited or were found to be inappropriate, active flow control (AFC) may lead to additional improvements in aerodynamic performance. A comprehensive analysis of the state of AFC (of the various conceptual approaches such as open-loop, closed-loop, and optimal control), together with a number of illustrative examples, was provided by Collis et al. [1]. In open-loop control, the controller parameters are determined a priori for a certain operating point and then kept constant during nominal operation. An efficient open-loop control can be obtained when instabilities of the flow are exploited. In closed-loop control, the actuation changes in response to changes in the flow. For robustness, closed-loop control should also be capable of compensating for disturbances (for example, as caused by gusts) to the system that are expected in the practical application. Uncertainties about the flow dynamics (in control theory, *plant dynamics*) or disturbances entering the system make controller design difficult. When synthesizing a controller, a compromise is sought between robust stability, disturbance rejection, and control energy requirements. These requirements are met by $\mathcal{H}_\infty$ methods (robust optimal control) [2,3]. $H_\infty$ algorithms have no real-time capability and therefore cannot be directly employed for flow control. They may, however (through appropriate model simplification/reduction techniques), lead to simplified models that are suitable for real-time control.

The idea of basing controller design on reduced-order models (ROMs) of the flow (Galerkin models, vorticity models, etc.) seems to be promising [4–9]. The term *reduced order* indicates that these models are based on a truncated model basis. However, stable ROMs that are appropriate for controller design purposes have only been derived for a few simple flows (e.g., circular cylinder or

Presented as Paper 1403 at the 44th AIAA Aerospace Sciences Meeting and Exhibit, Reno, NV, 9–12 January 2006; received 26 January 2006; revision received 28 August 2006; accepted for publication 12 December 2006. 

*Research Assistant Professor. Member AIAA.
†Professor. Member AIAA.

rectangular cavity). A ROM that describes the circular cylinder wake for two operating points [namely, the (unstable) symmetric steady state and the time-periodic vortex shedding] was developed by Noack et al. [7–9]. The model was based on a proper orthogonal decomposition (POD) of the unsteady flow. A shift mode was added that describes the difference between operating points 1 and 2. Global stability analysis eigenmodes [10] (or biglobal modes, meaning that the instability of a two-dimensional basic state is studied [11]) were added to describe the flow dynamics close to operating point 1. An additional mode was added to the ROM that describes how the flow control (displacement of the cylinder normal to the freestream direction) enters the model. The mode shape was taken from a low Reynolds number steady-state solution of the cylinder with transverse velocity. The resulting model fairly well describes the dynamics of the flow in the vicinity of both operating points and the transient from one operating point to the other. A Galerkin model based exclusively on POD modes fails to reproduce the transient seen in the original Navier–Stokes data. Noack et al. [7] point out that although Galerkin models based on POD modes provide accurate and efficient representations of the reference flow, the price to pay for the low dimensionality is a lack of robustness when the model dynamics deviate from the reference data. This is attributed to an inherent structural instability of Galerkin models based purely on POD modes. The inclusion of stability eigenmodes (which, in the POD sense, include a vanishing amount of kinetic energy) was found to considerably improve the prediction of the transient dynamics.

In summary, the following important issues have to be addressed when considering ROMs based on POD modes:

1) Without additional modes, the model can reliably capture the flow dynamics only in close vicinity of the operating point for which it was designed. This, of course, is only acceptable if the controller influence on the dynamics of the flow is gradual and the POD basis is updated repetitively [12] during the process.

2) The complexity of the flow dynamics determines the number of required modes. Low-order ROMs will work better for flows that are governed by energetic flow structures.

3) When ROMs are based on a truncated modal basis, modeling of the interaction of the resolved modes with the neglected higher-order modes and the energy dissipation of the higher-order modes [13–16] may result in better model accuracy and robustness.

4) Models built from fewer modes appear to be more disturbance-tolerant, but they lack diffusion and may reach unrealistically large limit cycle amplitudes. Models built from a large number of modes appear to be very sensitive to deviations from the design operating point (due to their inherent structural instability [7]).

5) The inclusion of global stability analysis eigenmodes can drastically improve the model prediction of flow transients [17].

6) For a ROM to be useful for controller design, it needs to capture more than one operating point and also model the interaction of the control input with the flow dynamics. Especially when the interaction of the flow control with the flow is complicated, it is not clear how the control (actuation) enters the ROM equations.

In the present paper, ROMs based on POD eigenmodes are analyzed. For simplicity, both the modal basis and the ROM are developed assuming incompressible flow. For the low Mach number flows considered in this paper, the circular cylinder flow and a more complex flow (the flow through a linear low-pressure turbine (LPT) cascade [12,18]), this assumption is justified. Results are shown for standard Galerkin models and for models in which all model coefficients are determined from a pure optimization procedure. The advantages of both approaches can be combined when the Galerkin model coefficients are calibrated using the procedure proposed by Couplet et al. [15], resulting in more accurate models with better long-time behavior. In addition, several other novel ideas for calibrating the Galerkin coefficients based on physical reasoning are investigated. Then it is shown how ROMs can be expanded to include model coefficients that describe how the flow control affects the model dynamics. These coefficients are obtained by an error-minimization technique in which the transient (during which the flow adjusts to the change in control) is deliberately excluded. Therefore, the resulting models are (on purpose) not able to capture the transient from one operating point to the other. Finally, the performance of a composite ROM that includes POD modes from two operating points is evaluated.

## Modal Basis

Proper orthogonal decomposition results in a decomposition of the flow that captures most of its energy with the least number of modes [19]. For higher-dimensional problems, the snapshot method [20] is employed for computing the POD eigenmodes:

$$\mathbf{q}_i = \sum_{n=0}^{N} r_i^n \mathbf{v}^n \tag{1}$$

where the superscript $n = 0 \ldots N$ indicates the time step, $\mathbf{v}$ is the velocity vector, and $r_i$ are individual elements of $\mathbf{r}_i$, which are eigenvectors of the algebraic eigenvalue problem:

$$\mathbf{C}\,\mathbf{r}_i = \lambda_i \mathbf{r}_i \tag{2}$$

The correlation tensor $\mathbf{C}$ is defined as

$$C^{nn'} = \frac{1}{N+1}[\mathbf{v}^n(\mathbf{x}), \mathbf{v}^{n'}(\mathbf{x})]_\Omega \tag{3}$$

Here, the brackets denote the inner product:

$$(\mathbf{a}, \mathbf{b})_\Omega = \int_\Omega \mathbf{a}(\mathbf{x})^T \cdot \mathbf{b}(\mathbf{x})\, \mathrm{d}\mathbf{x} \tag{4}$$

The eigenfunctions can be normalized using their corresponding eigenvalues:

$$(\mathbf{q}_i, \mathbf{q}_{i'})_\Omega = \delta_{ii'}\lambda_i \tag{5}$$

and the time coefficients are computed as

$$a_i(t) = \frac{1}{\lambda_i}(\mathbf{v}(t), \mathbf{q}_i)_\Omega \tag{6}$$

POD modes that describe traveling coherent structures appear in pairs. The kinetic energy of the flow at a given time instant $t$ is

$$e(t) = \frac{1}{2}[\mathbf{v}(t), \mathbf{v}(t)]_\Omega = \frac{1}{2}\sum_i a_i^2(t)(\mathbf{q}_i, \mathbf{q}_i)_\Omega = \frac{1}{2}\sum_i a_i^2(t)\lambda_i \tag{7}$$

The time-averaged total kinetic energy of the flow is

$$\langle e(t) \rangle = \frac{1}{2}\sum_i \lambda_i \tag{8}$$

where $\langle a_i a_i \rangle = 1$ and the kinetic energy of the individual POD modes is $\lambda_i/2$. Here, the brackets indicate the time average over a time interval:

$$\langle \ldots \rangle = \frac{1}{T}\int_T \ldots \, \mathrm{d}t \tag{9}$$

From the eigenmodes and time coefficients, the original data can be reconstructed/recovered:

$$\mathbf{v}(\mathbf{x}, t) = \sum_{i=0}^{I} a_i(t)\mathbf{q}_i(\mathbf{x}) \tag{10}$$

The POD modes are orthogonal to each other and usually sorted according to their respective energy contents. For low Reynolds number flows, the dropoff in mode energy toward the higher mode numbers is typically significant and a small number of modes is sufficient for capturing a large percentage of the kinetic energy of the flow. This is also the case for higher Reynolds number flows when the flow dynamics are governed by large energetic structures of organized (or coherent) fluid motion.

The POD modal basis can accurately describe the dynamics of the flow only in close vicinity of the operating point for which it was derived. Additional modes may be added to make the model more versatile. These additional modes $\mathbf{q}_a$ can be made orthogonal to an existing orthogonal modal basis $\mathbf{q}_i$ $(i = 0, \ldots, I)$ via a Gram–Schmidt orthogonalization procedure:

$$\mathbf{q}'_a = \mathbf{q}_a - \sum_{i=0}^{I} \frac{(\mathbf{q}_a, \mathbf{q}_i)_\Omega}{\|\mathbf{q}_i\|_\Omega^2} \mathbf{q}_i \tag{11}$$

$$\mathbf{q}'_a \Leftarrow \frac{\mathbf{q}'_a}{\|\mathbf{q}'_a\|_\Omega} \tag{12}$$

where $\|\mathbf{q}_i\|_\Omega^2 = (\mathbf{q}_i, \mathbf{q}_i)_\Omega$.

If the model is to be used for control purposes, the control has to enter the model equations. This can be accomplished by adding a number of $J$ actuation modes. Following the suggestion by Noack et al. [8], negative indices are used for the actuation modes (which are unknown) and the actuation time coefficients (which are prescribed and thus known):

$$\mathbf{v}(\mathbf{x}, t) = \sum_{i=-J}^{I} a_i(t) \mathbf{q}_i(\mathbf{x}) \tag{13}$$

## Reduced-Order Model

### Derivation of ROM Equations

The modal decomposition [Eq. (10)] is inserted into the incompressible Navier–Stokes equations:

$$\frac{\partial}{\partial t}\mathbf{v} + \mathbf{v} \cdot \nabla \mathbf{v} + \nabla p = \frac{1}{Re} \Delta \mathbf{v} \tag{14}$$

resulting in

$$\sum_{j=-J}^{I} \frac{\partial a_j}{\partial t} \mathbf{q}_j + \sum_{j,k=-J}^{I} a_j a_k (\mathbf{q}_j \cdot \nabla \mathbf{q}_k) + \nabla p - \frac{1}{Re} \sum_{j=-J}^{I} a_j \Delta \mathbf{q}_j = 0 \tag{15}$$

All modes satisfy the incompressibility condition $\nabla \cdot \mathbf{q}_j = 0$. The ROM system is obtained by a Galerkin projection of the Navier–Stokes equations onto the space spanned by the modal basis:

$$\sum_{j=-J}^{I} \frac{\partial a_j}{\partial t} (\mathbf{q}_j, \mathbf{q}_i)_\Omega + \sum_{j,k=-J}^{I} a_j a_k (\mathbf{q}_j \cdot \nabla \mathbf{q}_k, \mathbf{q}_i)_\Omega + (\nabla p, \mathbf{q}_i)_\Omega - \frac{1}{Re} \sum_{j=-J}^{I} a_j (\Delta \mathbf{q}_j, \mathbf{q}_i)_\Omega = 0 \tag{16}$$

The pressure term $(\nabla p, \mathbf{q}_i)$ is

$$(\nabla p, \mathbf{q}_i)_\Omega = \int_\Omega \nabla p \cdot \mathbf{q}_i \, \mathrm{d}\mathbf{x} = \int_{\partial\Omega} p \mathbf{q}_i \cdot \mathbf{n} \, \mathrm{d}\mathbf{x} - \int_\Omega p \nabla \cdot \mathbf{q}_i \, \mathrm{d}\mathbf{x} \tag{17}$$

Keeping in mind that $\nabla \cdot \mathbf{q}_i = 0$, the pressure term is zero if $\mathbf{q}_i \cdot \mathbf{n}$ is zero on the boundaries. Otherwise, the term represents the influence of the "outside world" (e.g., external disturbances) on the flow and has to be taken into account. However, it is usually neglected. For example, Noack et al. [21] show that disregarding the pressure term is justified for long wake domains. Because the actuation modes are specified by the controller, only the time-evolution equations for $i = 0 \ldots I$ need to be advanced in time:

$$\sum_{j=0}^{I} \tilde{m}_{ij} \frac{\partial a_j}{\partial t} = - \sum_{j,k=-J}^{I} \tilde{q}_{ijk} a_j a_k + \frac{1}{Re} \sum_{j=-J}^{I} \tilde{l}_{ij} a_j - \sum_{j=-J}^{-1} \tilde{f}_{ij} \frac{\mathrm{d}a_j}{\mathrm{d}t} \tag{18}$$

where $\tilde{m}_{ij} = (\mathbf{q}_j, \mathbf{q}_i)_\Omega$ $(\delta_{ij}\lambda_i$ for the POD base), $\tilde{q}_{ijk} = (\mathbf{q}_j \cdot \nabla \mathbf{q}_k, \mathbf{q}_i)_\Omega$, $\tilde{l}_{ij} = (\Delta \mathbf{q}_j, \mathbf{q}_i)_\Omega$, and $\tilde{f}_{ij} = (\mathbf{q}_j, \mathbf{q}_i)_\Omega$. If the actuation modes are orthogonal to the modal base, the forcing coefficients $\tilde{f}_{ij}$ are zero and the actuation time coefficients enter the ROM equations only through the convective and viscous terms. Multiplication of the system with the inverse of matrix $\tilde{m}_{ij}$ yields

$$\frac{\partial a_i}{\partial t} = - \sum_{j,k=-J}^{I} q_{ijk} a_j a_k + \frac{1}{Re} \sum_{j=-J}^{I} l_{ij} a_j - \sum_{j=-J}^{-1} f_{ij} \frac{\mathrm{d}a_j}{\mathrm{d}t} \tag{19}$$

for $i = 0 \ldots I$ with $q_{ijk} = \sum_{l=1}^{I} \tilde{m}_{il}^{-1} \tilde{q}_{ljk}$, $l_{ij} = \sum_{l=1}^{I} \tilde{m}_{il}^{-1} \tilde{l}_{lj}$, and $f_{ij} = \sum_{l=1}^{I} \tilde{m}_{il}^{-1} \tilde{f}_{lj}$. Because of the model truncation to $I$ modes, part of the energy transfer from the lower (more energetic) modes to the higher (less energetic) modes is artificially removed from the system. Aubry et al. [13] included cubic terms to account for the stabilizing effect of the Reynolds stresses. The cubic terms were derived for a turbulent boundary layer in which the governing equations were spatially filtered and the Reynolds stress was computed with a subgrid stress turbulence model. Similar thoughts led Ukeiley et al. [14] to the inclusion of cubic terms into their model for a plane turbulent mixing layer. In generalized form, ROMs can be written as a system of $i = 0 \ldots I$ equations [22]:

$$\frac{\partial a_i}{\partial t} + \sum_{j=-J}^{I} l_{ij} a_j + \sum_{j=-J}^{I} \sum_{k=-J}^{j} q_{ijk} a_j a_k + \sum_{j=-J}^{I} \sum_{k=-J}^{j} \sum_{l=-J}^{k} c_{ijkl} a_j a_k a_l + \sum_{j=-J}^{-1} f_{ij} \frac{\mathrm{d}a_j}{\mathrm{d}t} = 0 \tag{20}$$

Each equation has $N = I + 1 + J$ linear coefficients, $[(N + 1)N]/2$ quadratic coefficients, $(N^3 + 3N^2 + 2N)/6$ cubic coefficients, and $J$ forcing coefficients.

### Error-Minimization Technique for Determining Model Coefficients

If the time coefficients $a_i$ $(i = 0 \ldots I)$ and control inputs $a_i$ $(i = -J \ldots -1)$ are known for a given time interval, all or some of the ROM coefficients can be determined by minimizing the time-averaged square of the left-hand side (LHS) of Eq. (20):

$$E = \left\langle \sum_{i=1}^{I} (\text{LHS of Eq. } 20)^2 \right\rangle \tag{21}$$

This is equivalent to employing a least-squares method for fitting the model coefficients [22,23]. Taking $\partial E / \partial l_{ij} \stackrel{!}{=} 0$ results in $\langle 2 a_j (\text{LHS of Eq. } 20) \rangle = 0$, taking $\partial E / \partial q_{ijk} \stackrel{!}{=} 0$ leads to $\langle 2 a_j a_k (\text{LHS of Eq. } 20) \rangle = 0$, taking $\partial E / \partial c_{ijkl} \stackrel{!}{=} 0$ results in $\langle 2 a_j a_k (\text{LHS of Eq. } 20) \rangle = 0$, and taking $\partial E / \partial f_{ij} \stackrel{!}{=} 0$ leads to $\langle 2 \dot{a}_j (\text{LHS of Eq. } 20) \rangle = 0$. The resulting linear system of equations is solved to obtain the model coefficients.

### POD of Disturbance Quantities

In most instances, the POD mode 0 (the most energetic mode) is almost identical to the time average of the flow, and the corresponding time coefficient $a_0$ is approximately one. If $a_0 = 1$ is imposed, $\partial a_0 / \partial t = 0$, and the time-evolution equation for mode 0 does not need to be integrated in time. This can be achieved by feeding only the time-dependent part of the flow data (the disturbance quantities)

$$\mathbf{v}' = \mathbf{v} - \bar{\mathbf{v}} = \mathbf{v} - \frac{1}{N+1} \sum_{n=0}^{N} \mathbf{v}^n \tag{22}$$

into the POD. This results in the decomposition

$$\mathbf{v}(\mathbf{x}, t) = \sum_{i=0}^{I} a_i(t) \mathbf{q}_i(\mathbf{x}) \tag{23}$$

where $a_0 = 1$, $a_i^n = 1/\lambda_i(\mathbf{v}^n - \bar{\mathbf{v}}, \mathbf{q}_i)$, and $\mathbf{q}_0 = \bar{\mathbf{v}}$. For this particular choice, $\mathbf{q}_0$ is not orthogonal to the remaining modes. Because $\partial a_0/\partial t = 0$, the resulting ROM is

$$\frac{\partial a_i}{\partial t} + \sum_{j=-J}^{I} l_{ij} a_j + \sum_{j=-J}^{I} \sum_{k=-J}^{j} q_{ijk} a_j a_k + \sum_{j=-J}^{-1} f_{ij} \frac{\mathrm{d}a_j}{\mathrm{d}t} = 0 \quad (24)$$

for $i = 1 \ldots I$. Because $a_0 = 1$, the model can also be written in a more compact form:

$$\frac{\partial a_i}{\partial t} + \sum_{j=-J}^{I} \sum_{k=-J}^{j} q'_{ijk} a_j a_k + \sum_{j=-J}^{-1} f_{ij} \frac{\mathrm{d}a_j}{\mathrm{d}t} = 0 \quad (25)$$

where

$$q'_{ijk} = \begin{cases} l_{ij} + q_{ijk} & \text{if } k = 0 \\ q_{ijk} & \text{otherwise} \end{cases} \quad (26)$$

It should be noted that a rigorous extension of both the POD and the Galerkin projection to compressible flows shows that the resulting ROMs are quadratic in both the convective and viscous terms [24,25]. Therefore, a ROM as represented by Eq. (25) would also be appropriate for describing compressible flows.

**Calibrated ROMs**

There are a number of other possible explanations for the sometimes poor performance of ROMs obtained from a Galerkin projection on POD modes, aside from their limited robustness due to their inherent structural instability [7,17]. The model deficiencies may be attributed to 1) a lack of accuracy when computing the coefficients of the Galerkin system (due to numerical accuracy, assumption of incompressible flow, etc.), 2) the model truncation (energy is dissipated in the small scales; the neglect of higher modes leads to reduced damping), and 3) an inaccurate treatment of the boundary terms (neglecting the pressure term; an observation window that does not encompass entire flow). Couplet et al. [15] have demonstrated that a full optimization of all model coefficients can lead to ill-conditioned, unstable ROMs. Therefore, they suggested a calibration procedure for the ROM coefficients that greatly improves the model accuracy while keeping the model well-conditioned. ROMs obtained from a Galerkin projection can be written as

$$\dot{\mathbf{a}} + \mathbf{f} = 0 \quad \text{with } \mathbf{f} = \sum_{k=0}^{P} \mathbf{y}_k m_k \quad (27)$$

where the vector $\mathbf{y}_k$ contains the model coefficients $l_{ij}$ and $q_{ijk}$. For two modes ($M = 2$), the monomial basis has $P = 1 + M + M(M + 1)/2 = 6$ elements ($m_1 = 1$, $m_2 = a_1$, $m_3 = a_2$, $m_4 = a_1^2$, $m_5 = a_1 a_2$, and $m_6 = a_2^2$). Each $\mathbf{y}_k$ has $M$ elements. If all coefficients in $\mathbf{y}$ are sought, the total number of unknowns is $M \cdot P = 12$. The general idea is to minimize the weighted average ($\alpha \in [0, 1]$):

$$\mathcal{J} = (1 - \alpha)\mathcal{E} + \alpha\mathcal{D} \quad (28)$$

where $\mathcal{E}$ is a measure of how well the calibrated system fits the given or experimental time coefficients and $\mathcal{D}$ is a measure of the difference between the coefficients of the calibrated system $\mathbf{y}^\alpha$ and the coefficients obtained form the Galerkin projection $\mathbf{y}^g$. For $\alpha = 0$, the calibrated system is fully optimized but ill-conditioned. For $\alpha = 1$, the original coefficients from the Galerkin projection are recovered. The errors can be quantified in a normalized form as

$$\mathcal{E} = \frac{\langle \|\mathbf{e}(\mathbf{y}, t)\|^2 \rangle}{\langle \|\mathbf{e}(\mathbf{y}^g, t)\|^2 \rangle} \quad \text{and} \quad \mathcal{D} = \frac{\|\mathbf{y} - \mathbf{y}^g\|^2}{\|\mathbf{y}^g\|^2} \quad (29)$$

Couplet et al. [15] proposed three error definitions. For the results presented here, the third definition,

$$\mathbf{e}(\mathbf{y}^\alpha, t) = \dot{\mathbf{a}}^e(t) + \mathbf{f}^\alpha[\mathbf{a}^e(t)] \quad (30)$$

was employed. With this definition and $\alpha = 0$, the calibration procedure becomes identical to Eq. (21). Linearization of the error in terms of $\mathbf{y}$ leads to

$$\mathbf{e}(\mathbf{y}, t) = \mathbf{e}(0, t) + \frac{\partial \mathbf{f}}{\partial \mathbf{y}} \mathbf{y} = \mathbf{e}(0, t) + \mathbf{E}(t)\mathbf{y} \quad (31)$$

The norms are

$$\langle \|\mathbf{e}(\mathbf{y}, t)\|^2 \rangle = \langle \mathbf{e}(0, t)^T \mathbf{e}(0, t) \rangle + 2\langle \mathbf{E}(t)^T \mathbf{e}(0, t) \rangle^T \mathbf{y} + \mathbf{y}^T \langle \mathbf{E}(t)^T \mathbf{E}(t) \rangle \mathbf{y} = c + 2\mathbf{l}\mathbf{y} + \mathbf{y}^T \mathbf{A} \mathbf{y} \quad (32)$$

$$\|\mathbf{y} - \mathbf{y}^g\|^2 = \mathbf{y}^T\mathbf{y} - 2\mathbf{y}^T\mathbf{y}^g + \mathbf{y}^{gT}\mathbf{y}^g \quad (33)$$

The minimum of Eq. (28) is found from

$$\frac{\partial \mathcal{J}}{\partial \mathbf{y}} = \chi_A(2\mathbf{A}\mathbf{y} + 2\mathbf{l}) + \chi_\Pi(2\mathbf{y} - 2\mathbf{y}^g) \stackrel{!}{=} 0 \quad (34)$$

with

$$\chi_A = \frac{1 - \alpha}{\langle \|\mathbf{e}(\mathbf{y}^g, t)\|^2 \rangle} = \frac{1 - \alpha}{\langle [\dot{\mathbf{a}}^e + \mathbf{f}^g(\mathbf{a}^e)]^T [\dot{\mathbf{a}}^e + \mathbf{f}^g(\mathbf{a}^e)] \rangle} \quad (35)$$

$$\chi_\Pi = \frac{\alpha}{\mathbf{y}^{gT}\mathbf{y}^g} = \frac{\alpha}{\sum {l_{ij}^g}^2 + \sum {q_{ijk}^g}^2} \quad (36)$$

or, in short,

$$(\chi_A \mathbf{A} + \chi_\Pi \mathbf{I})\mathbf{y} = (-\chi_A \mathbf{l} + \chi_\Pi \mathbf{y}^g) \quad (37)$$

$$\mathbf{B}^\alpha \mathbf{y} = \mathbf{l}^\alpha \quad (38)$$

The resulting $k = 1 \ldots M$ uncoupled linear systems of equations, with $P$ unknowns each, are then solved for the coefficients of the calibrated system $\mathbf{y}$. Individual elements of $\mathbf{A}$ are $\mathbf{A}_{i,j} = \langle m_i[\mathbf{a}^e(t)]^T m_j[\mathbf{a}^e(t)] \rangle$. Individual elements of $\mathbf{l}$ are $\mathbf{l}_{k,i} = \langle m_i[\mathbf{a}^e(t)]^T \dot{a}_k^e(t) \rangle$.

**Other ROM Calibration Procedures**

The change in mode energy $e_i = 1/2\langle a_i a_i \rangle$ over a characteristic time interval is

$$\frac{e_i(T) - e_i(0)}{T} = \left\langle \frac{\partial e_i}{\partial t} \right\rangle = \left\langle a_i \frac{\partial a_i}{\partial t} \right\rangle = -\sum_j \langle a_i a_j \rangle l_{ij} - \sum_{j,k} \langle a_i a_j a_k \rangle q_{ijk} - \sum_j \langle a_i \dot{a}_j \rangle f_{ij} \quad (39)$$

Here, the time coefficients are normalized as $\langle a_i a_{i'} \rangle = \delta_{ii'} \lambda_i$. If the calibrated model had the same change in mode energy as the Galerkin model, the error

$$\sum_j \langle a_i a_j \rangle \left( l_{ij} - l_{ij}^g \right) + \sum_{j,k} \langle a_i a_j a_k \rangle \left( q_{ijk} - q_{ijk}^g \right) + \sum_j \langle a_i \dot{a}_j \rangle f_{ij} \stackrel{!}{=} \mathbf{g}^T(\mathbf{y} - \mathbf{y}^g) \quad (40)$$

would be identical zero. The normalized square of the error is

$$\mathcal{D} = \frac{(\mathbf{y} - \mathbf{y}^g)^T \mathbf{g}\mathbf{g}^T (\mathbf{y} - \mathbf{y}^g)}{\mathbf{y}^{gT}\mathbf{g}\mathbf{g}^T\mathbf{y}^g} \quad (41)$$

For $\mathbf{g}\mathbf{g}^T = \mathbf{I}$, this expression becomes identical to the second expression in Eq. (29). Corrected model coefficients are obtained by seeking a minimum of $\mathcal{D}$:

$$\frac{\partial \mathcal{D}}{\partial \mathbf{y}} = \frac{\mathbf{g}\mathbf{g}^T}{\mathbf{y}^{gT}\mathbf{g}\mathbf{g}^T\mathbf{y}^g}(2\mathbf{y} - 2\mathbf{y}^g) \stackrel{!}{=} 0 \tag{42}$$

and solving the resulting system of equations. Minimizing the energy change of the individual modes results in

$$\frac{\mathbf{g}\mathbf{g}^T}{\mathbf{y}^{gT}\mathbf{g}\mathbf{g}^T\mathbf{y}^g} 2\mathbf{y} \stackrel{!}{=} 0 \tag{43}$$

Especially in the presence of external forcing, cases may exist in which individual modes are gaining energy while others are losing energy over a given time interval. Enforcing a zero net change in total energy or minimization of $\sum_i \langle \partial e_i / \partial t \rangle$ leads to

$$\frac{2\mathbf{g}_i \sum_j \mathbf{g}_j^T \mathbf{y}_j}{\left(\sum_j \mathbf{g}_j^T \mathbf{y}_j^g\right)^2} \stackrel{!}{=} 0 \tag{44}$$

The model truncation interrupts the energy transfer from the lower, more energetic resolved modes to the higher, less energetic (now unresolved) dissipative modes. One may account for the missing energy transfer by scaling the viscous terms with a parameter $\nu_i$. Defining an error as

$$E = \left\langle \sum_i \left( \dot{a}_i + \nu_i \sum_j l_{ij} a_j + \sum_{j,k} q_{ijk} a_j a_k \right)^2 \right\rangle \tag{45}$$

and taking $\partial E / \partial \nu_i \stackrel{!}{=} 0$ results in

$$\nu_i = -\frac{\langle (\dot{a}_i + \sum_{j,k} q_{ijk} a_j a_k)(\sum_j l_{ij} a_j) \rangle}{\langle (\sum_j l_{ij} a_j)^2 \rangle} \tag{46}$$

This approach has a similar effect as the spectral viscosity method by Sirisup and Karniadakis [16], which amounts to multiplying the viscous terms by a factor of $1 + \varepsilon \hat{Q}_i$, where $\hat{Q}_i$ is the viscosity kernel, defined as

$$\hat{Q}_i = \begin{cases} 0 & \text{if } i \le M \\ 1 & \text{otherwise} \end{cases} \tag{47}$$

with cutoff mode number $M$. The parameter $\varepsilon$ is a viscosity amplitude that can be made dependent on the number of modes included in the model $\varepsilon = \alpha / I$. For the spectral viscosity approach, both the cutoff mode number and the parameter $\alpha$ are adjustable parameters.

In some instances, the following approach for including an actuation mode into a ROM may work [26]. A steady solution of the flow $\mathbf{q}_{-1}$ is computed with steady control/forcing input $a_{-1} = 1$. Then a simulation with time-dependent forcing input $a_{-1}(t)$ is performed. The forcing signal is subtracted from the time-dependent data:

$$\tilde{\mathbf{v}}(t) = \mathbf{v}(t) - a_{-1}(t)\mathbf{q}_{-1} \tag{48}$$

where $\tilde{\mathbf{v}}(t)$ has homogeneous boundary conditions at the actuator location. A POD of $\tilde{\mathbf{v}}$ yields the POD modes $\tilde{\mathbf{q}}$. By taking the time derivative of Eq. (48) and substituting $\partial \mathbf{v} / \partial t$ with the right-hand side of the Navier–Stokes equations and then performing a Galerkin projection of the resulting equations on the $\tilde{\mathbf{q}}$ modal basis, a ROM with time-dependent control input is obtained. However, this approach is unfeasible for the applications discussed in this paper, because the flow structures that arise as a consequence of the unsteady forcing cannot be obtained from a steady-state solution.

An analogous procedure may be considered in which the effect of the forcing on the flow is obtained from an unsteady simulation with harmonic control input $a_{-1}$. The control input $a_{-1}$ can be related to the time signal of the first two POD modes with time coefficients $a_1(a_{-1})$ and $a_2(a_{-1})$ of the time-dependent flow data $\mathbf{v}(t)$. By subtracting the resulting modes 1 and 2 from the time-dependent flow data

$$\tilde{\mathbf{v}}(t) = \mathbf{v}(t) - a_1[a_{-1}(t)]\mathbf{q}_1 - a_2[a_{-1}(t)]\mathbf{q}_2 \tag{49}$$

and performing a POD on the modified data $\tilde{\mathbf{v}}$, modes $\tilde{\mathbf{q}}$ are obtained. A ROM with time-dependent control input is obtained by taking the time derivative of Eq. (49) and performing a Galerkin projection of the resulting equations on the $\tilde{\mathbf{q}}$ POD modes. This approach was not investigated further, because a principal shortcoming of this approach is that the actuation modes are dependent on the operating conditions (e.g., Reynolds number) and on the actuation itself. For the circular cylinder wake, it was shown that a ROM based on POD modes is valid only for a very small Reynolds number range [27]. Analogously, the flow dynamics can be captured sufficiently well by a given modal basis only for small changes in the actuation. Because of the aforementioned complications, models that describe the transient from the uncontrolled to the controlled flow and models that describe operating points that are noticeably different from each other were deliberately excluded in the following investigations.

## Results

### Flow Topologies

The accuracy and robustness of the various modeling approaches was first evaluated for time-dependent flow data obtained from compressible Navier–Stokes simulations of a circular cylinder at $Re = 100$ based on the cylinder diameter. The computational domain was discretized with two grid blocks of dimension $160 \times 60$ and $160 \times 78$ (Fig. 1a). The computed Strouhal number was 0.163. Data obtained from simulations of a linear LPT cascade operated at a Reynolds number (based on $C_x$) of 25,000 [12,18] were employed as well. Compared with the original experiments [28], the blade spacing was enlarged by 25% to increase the size of the separated flow region and thus make the flowfield more amenable to control. The computational domain was split into five grid blocks, with dimensions $20 \times 30$, $20 \times 20$, $500 \times 100$, $260 \times 100$, and $130 \times 110$ (Fig. 1b). The LPT flow was controlled by harmonic wall-normal blowing, $a_{-1} = 0.1[1 + \cos(2\pi F^+ t)]$, with an amplitude of 0.2 (nondimensionalized with the inflow velocity), and different forcing frequencies (nondimensionalized with inflow velocity and axial chord) through a slot (width $0.01 C_x$) located at 58% axial chord. The primary interest was to find robust ROMs that accurately describe the separated flow region (laminar separation bubble on the suction side of the blade) that is completely contained in the center block. Therefore, only flow data from the center block were used for the following investigations.

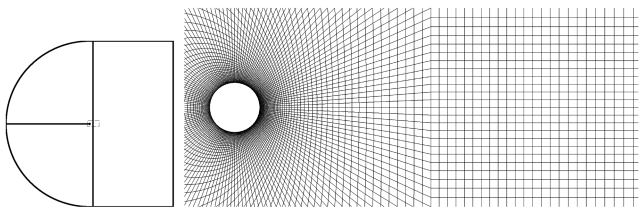

a)

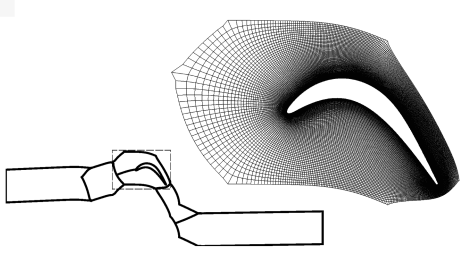

b)

**Fig. 1 Block boundary outlines and details of computational grids employed for simulations of a) circular cylinder and b) LPT flow (only the center grid is shown for the LPT geometry).**

**Discretization**

Derivatives associated with the Galerkin projection were computed with central finite differences of second-order accuracy. An explicit, fourth-order-accurate, four-stage Runge–Kutta scheme was used for advancing the ROM equations forward in time. A time-step study showed that the step sizes chosen for the results shown in this paper ($\Delta t = 0.01$ for the circular cylinder flow and $\Delta t = 0.001$ for the LPT flow) were sufficiently small. Time averages were computed using the second-order-accurate trapezoidal rule. For comparison and validation, the highly accurate Romberg integration was also employed for computing the time averages (not shown). Results obtained with both integration schemes were virtually identical.

**Modal Basis**

Time-dependent flow data from 500 snapshots at evenly spaced time intervals over a time horizon of $\Delta T = 20$ for the circular cylinder ($20 \times 0.163 = 3.3$ shedding cycles) and $\Delta T = 1$ for the LPT blade ($1 \times 5 = 5$ shedding cycles for the controlled flow with $F^+ = 5$) were used for the POD. The difference between the results obtained from the POD of the total velocities and the POD of the disturbance velocities was found to be minimal. Because inaccuracies are introduced into the ROM if $a_0$ is not exactly equal to one, all POD results in the remaining part of this paper were computed from the disturbance velocities.

Results for the circular cylinder are shown in Fig. 2. The eigenvalues of the lower modes ($i \leq 10$) appear in pairs of almost equal magnitude. The corresponding time coefficients and eigenmodes have similar shapes, but appear phase-shifted by 90 deg. Such mode pairs describe traveling waves. The mode energy dropoff toward the higher mode numbers is considerable. When the time coefficients are plotted against each other, they form closed trajectories, indicating the time-periodic nature of the flow.

In contrast, the time signals obtained from a POD of the uncontrolled LPT flow are not time-periodic (Fig. 3). The time interval chosen for the POD may have been too short for including enough characteristic time periods of the structures with the lowest relevant frequencies. However, eigenmodes 1 and 2 show a periodic pattern and their time signals are almost periodic. The trajectories of the higher mode number time coefficients are more or less chaotic. The picture changes noticeably when the LPT flow is subjected to harmonic forcing with $F^+ = 5$ (Fig. 4). The POD results indicate that the flow becomes time-periodic; the flow "locks in" to the forcing signal. The time-coefficient trajectories form closed loops and the eigenmodes show regular patterns. Eigenmodes 1 and 2 through 7 and 8 appear in pairs of equal magnitude. The corresponding eigenmodes and time coefficients are almost identical, apart from a phase shift of 90 deg. Again, these pairs constitute traveling waves. The frequency of the time coefficients of modes 1 and 2 corresponds to the forcing frequency; these modes are referred to as *fundamental* modes. Modes 3 and 4 and modes 5 and 6 describe the first and second higher harmonics of the actuation frequency (fundamental). Comparing results for the uncontrolled and controlled LPT flow, it becomes clear that the dropoff in mode energy is considerably more pronounced for the controlled flow than for the uncontrolled flow. For a given number of modes, a ROM of the controlled (and therefore more organized) flow will capture more of the kinetic energy and therefore represent the flow more accurately than a ROM of the uncontrolled (and more stochastic) flow.

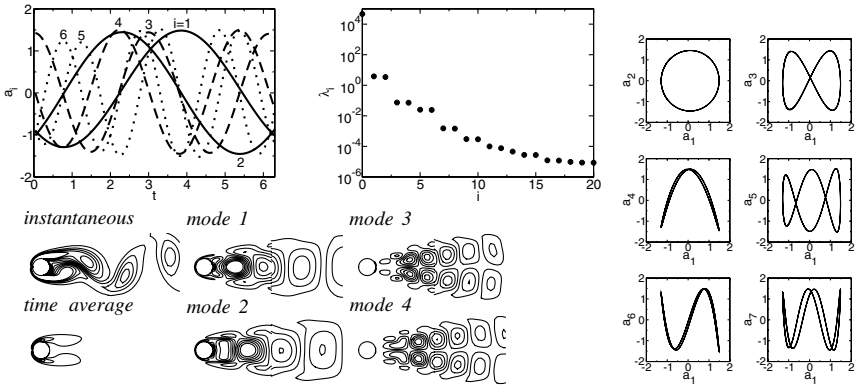


**Fig. 2 POD of circular cylinder flow; time coefficients, eigenvalues, and isocontours of vorticity for instantaneous flow, time average, and the first four POD modes.**

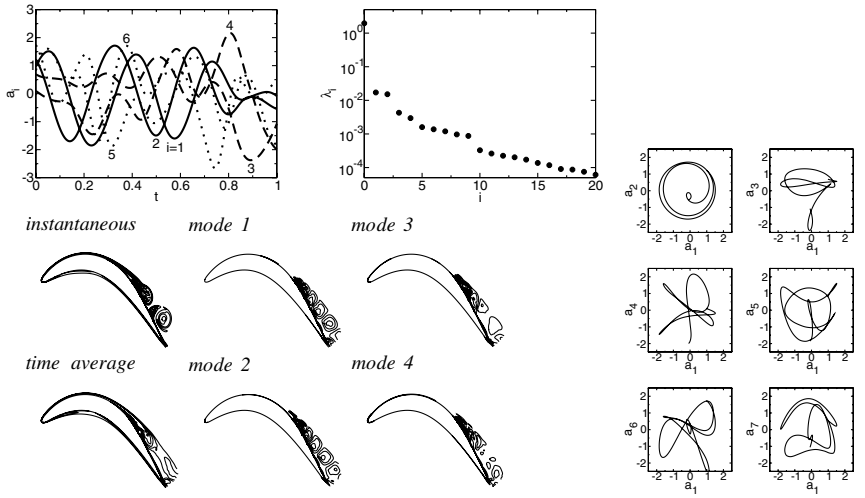


**Fig. 3 POD of uncontrolled LPT flow; time coefficients, eigenvalues, and isocontours of vorticity for instantaneous flow, time average, and the first four POD modes.**

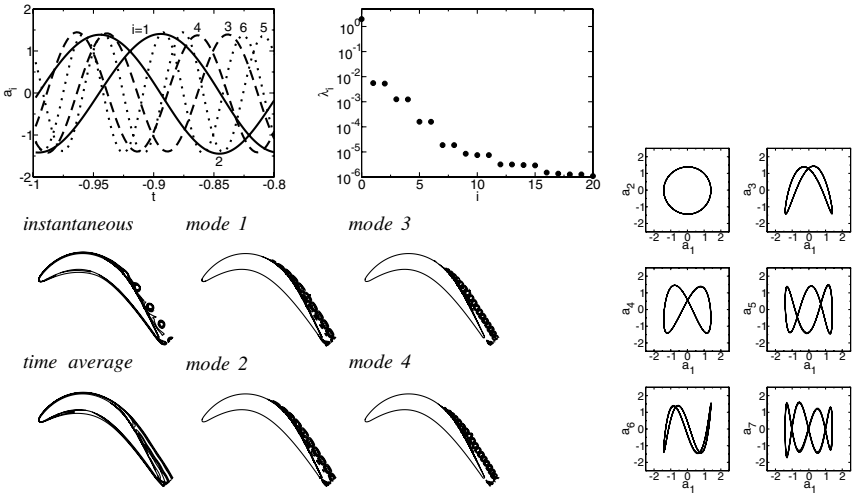


**Fig. 4 POD of controlled LPT flow ($F^+ = 5$); time coefficients, eigenvalues, and isocontours of vorticity for instantaneous flow, time average, and the first four POD modes.**

**ROMs with Coefficients Obtained from a Galerkin Projection**

Several reduced-order models with $I = 2$, 4, 8, 16, and 32 modes were derived from a Galerkin projection of the governing equations on the respective POD modal basis. The ROM model equations were then integrated forward in time over the time interval for which the modal basis was generated, and the time coefficients were then compared with the known (reference) time coefficients [obtained by projection of the flow data on the modal basis, Eq. (6)]. Results are shown in Fig. 5. Here, only the time coefficient for mode 1 is shown. The behavior of the time coefficient for mode 2 is qualitatively similar and does not provide additional information. Several observations can be made. The models seem to work considerably better for time-periodic flows (circular cylinder and controlled LPT flow) than for less organized flows (uncontrolled LPT flow). The dynamics of the geometrically less complicated low Reynolds number circular cylinder flow are captured more accurately than the dynamics of the higher Reynolds number controlled LPT flow. It should be mentioned that flow data from the entire computational domain were fed into the POD for the circular cylinder flow, whereas only data from the center block were used for the controlled LPT flow. Therefore, the error made by neglecting the boundary integral in the Galerkin projection can be expected to be larger for the controlled LPT flow. Numerical results for a cylinder wake by Noack et al. [21] support this conjecture. All models are relatively accurate near the beginning of the prediction time interval ($t = 0$) and then deviate more or less rapidly from the reference solution. Models with more modes are generally more accurate close to $t = 0$, but are considerably less robust. Minor deviations from the reference data are sufficient to cause a total destabilization of the model, hinting at the structural instability of pure Galerkin models. For POD models of the circular cylinder in particular, it is apparent that the higher POD modes drain energy from the lower POD modes. Neglecting the higher POD modes (model truncation) results in larger growth rates of the more energetic lower POD modes.

The ROM prediction of the dynamics of the uncontrolled LPT flow does not improve when the POD coefficients and eigenmodes are computed for a time interval that is twice as long ($\Delta T = 2$, not shown), thereby allowing the inclusion of more of the lower-frequency flow dynamics. An interesting feature of ROMs based on Galerkin models is that the effect of the Reynolds number can be investigated. For the circular cylinder, reducing the Reynolds number by a factor of 10 ($Re = 10$) results in significant damping of modes 3 and 4 (not shown) and marginal amplitude growth of modes 1 and 2 when compared with the $Re = 100$ results (Fig. 6a). The phase remains nearly unaffected. In experiments, the circular cylinder wake becomes unstable at $Re = 30 \ldots 40$ [29]. The difference between the $Re = 10$ results (based on the POD base for $Re = 100$) and the experimental observations can be attributed to the fact that the POD modes change significantly when the Reynolds

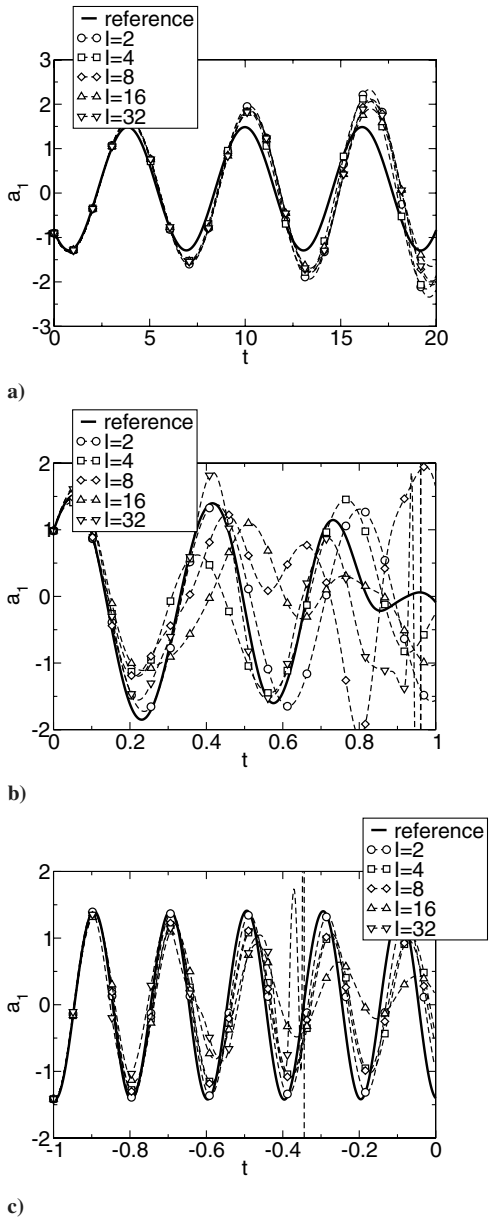


**Fig. 5 Comparison of ROM prediction with reference data; model coefficients from Galerkin projection: a) circular cylinder flow, b) uncontrolled LPT flow, and c) controlled LPT flow.**

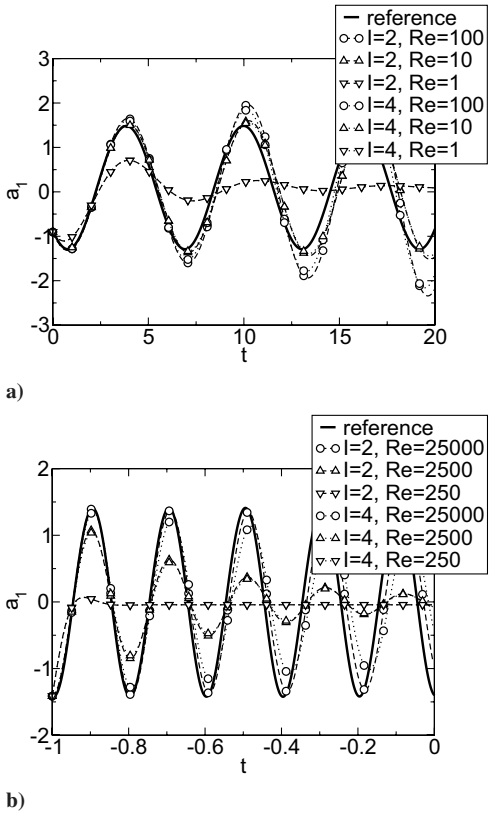


**Fig. 6 Effect of Reynolds number on ROM prediction; model coefficients from Galerkin projection: a) circular cylinder flow and b) controlled LPT flow.**

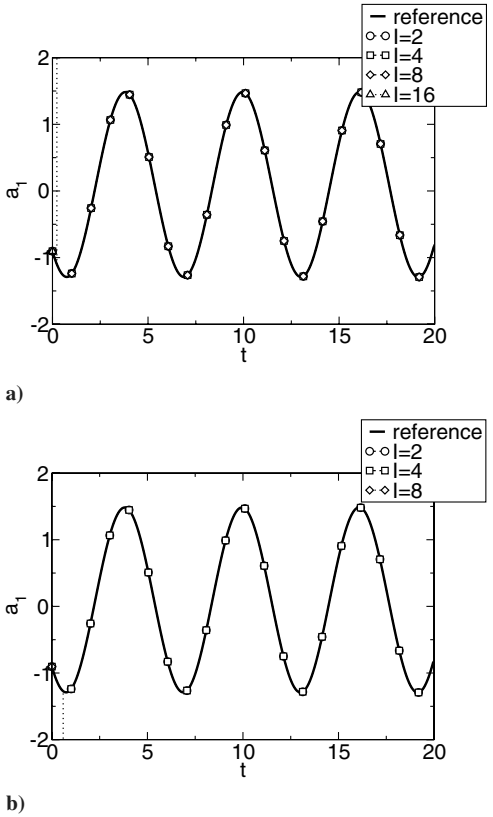


**Fig. 7 ROMs of circular cylinder flow; model coefficients from error-minimization; ROMs with a) linear and quadratic terms and b) linear, quadratic, and cubic terms.**

number is altered [27]. This is not reflected in the current approach. When the Reynolds number is further reduced by a factor of 10 ($Re = 1$), all mode amplitudes are strongly dampened (the oscillation amplitudes are decaying quickly) and the system approaches a steady state ($a_i \approx 0$ for $i = 1, \ldots I$). A similar behavior can be observed for the controlled LPT flow (Fig. 6b). The model with four modes is damped more strongly than the model with two modes when the Reynolds number is lowered by a factor of 10 ($Re = 2500$). When the Reynolds number is lowered even further, the time coefficients approach a steady state that is not identical zero. The steady-state solution of the ROM is not identical to the time average of the simulation data.

#### ROMs with Coefficients Obtained from Error-Minimization

In contrast to the results from the previous approach, when all model coefficients are obtained from the error-minimization technique, quadratic ROMs of the circular cylinder flow with 2, 4, and 8 modes track the reference solution very accurately, as shown in Fig. 7a. The resulting models are henceforth also referred to as (fully) optimized models. The quadratic model with 16 modes becomes unstable very early on and deviates rapidly from the reference solution. This rapid deviation can be interpreted as an extreme sensitivity of the model with respect to disturbances, indicating that the model robustness is minimal. Inclusion of cubic terms makes the models even less robust and hardly increases accuracy. It should be kept in mind that the error-minimization technique does not use the coefficients obtained from the Galerkin projection. Although models based on a Galerkin projection may capture the dynamics and energy fluxes of the real flow [30], models solely derived from an optimization do not. Fully optimized models of the uncontrolled LPT flow perform even worse with respect to robustness (not shown).

It can be concluded that ROMs based on a full optimization of the model coefficients can be very accurate (when they work), but they lack robustness and are therefore not suited for control problems in which disturbances must be tolerated. When the model coefficients are fully optimized, the internal structure of the ROM is not based on physics (in contrast to Galerkin models). This becomes apparent when the model Reynolds number is lowered [31]. Fully optimized models are very sensitive to disturbances (they are ill-conditioned) and react erratically to Reynolds number changes. One may consider combining the robustness of the Galerkin model with the accuracy of the optimization procedure by retaining the linear and quadratic terms from the Galerkin projection and obtaining the cubic terms from an optimization. However, in our preliminary investigations, this procedure did not lead to more robust models (results not shown).

#### Calibrated ROMs

A good balance between accuracy and robustness is achieved when the calibration procedure by Couplet et al. [15] is employed. For $\alpha = 0$, the coefficients are fully optimized, and for $\alpha = 1$, the original coefficients from the Galerkin projection are recovered. The suggested calibration or weighing parameter $\alpha$ is 0.05. The resulting ROMs work very well for the two time-periodic flows (circular cylinder and controlled LPT flow, Fig. 8a and 8c). Models with up to 32 modes show robust behavior over the entire integration time interval. For the more chaotic uncontrolled LPT flow, models with two and four modes do not follow the reference solution. Models with 16 and 32 modes capture the flow dynamics surprisingly well.

The question of how the calibration procedure affects the quadratic terms in the ROM for the circular cylinder can be answered when resorting to Fig. 9. The original quadratic coefficients obtained from the Galerkin projection, $q^g_{ijk}$ ($j, k = 0 \ldots I$), are visualized in the top row. The second row shows the coefficients $q_{ijk} = q^g_{ijk} + q^g_{ikj}$ ($j = 0 \ldots I, k = 0 \ldots j$), and the third row shows the coefficients $q_{ijk}$ as obtained from the calibration with $\alpha = 0.05$. The calibration corrects the individual coefficients only slightly and does not noticeably alter the structure (which, for the quadratic coefficients, describes the convective mode interaction) of the model. This may explain why the calibrated model is almost as robust as the Galerkin

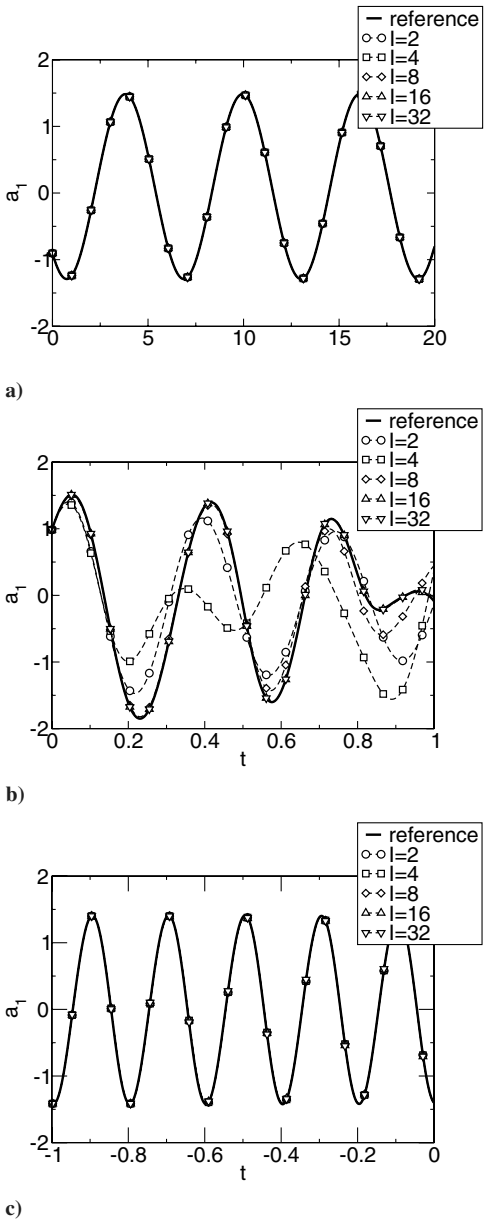


**Fig. 8 Calibrated ROMs with $\alpha = 0.05$: a) circular cylinder flow, b) uncontrolled LPT flow, and c) controlled LPT flow.**

model and why the calibrated model shows a behavior similar to the Galerkin model when the Reynolds number is altered [31]. When the model is fully optimized ($\alpha = 0$), the coefficients are changed radically and bear no resemblance to the coefficients of the original Galerkin model (bottom row of Fig. 9). In fact, the white and black boxes in the bottom row of the figure correspond to values that are far (up to two orders of magnitude) outside of the displayed range. This explains why slight deviations from the reference solution are strongly amplified, resulting in rapid and catastrophic failure of the model: the model is ill-conditioned. This also explains why the fully optimized model does not respond correctly to changes in the Reynolds number.

#### Other ROM Calibration Procedures

When the coefficients obtained from the Galerkin projection are modified such that the change in mode energy over a given time interval is identical to the change in mode energy for the original Galerkin model [Eq. (42)], model accuracy and robustness are only improved slightly [31]. One may instead choose to minimize the energy change for each individual mode [Eq. (43)] or to minimize the sum of the changes in modal energy [to enforce the modal energy

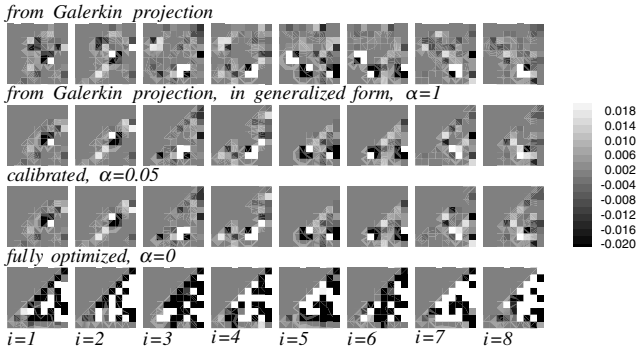


**Fig. 9 ROMs of circular cylinder flow with eight modes; Quadratic terms $q_{ijk}$ (abscissa: $j$, ordinate: $k$).**

flow balance, Eq. (44)] over the same time interval. Even when these objectives are achieved, the resulting models are neither more accurate nor more robust [31]. When the viscous terms of the ROMs are modified such that the energy change of the individual modes over the time interval is minimized [Eq. (46)], the viscous damping of modes 1 and 2 is increased by one order of magnitude for the circular cylinder flow, whereas the higher modes are affected less (Fig. 10a). Overall, the model accuracy is slightly improved. Similar observations can be made for the controlled LPT flow (Fig. 10b). For models with eight or less modes, the procedure results in more accurate models. For models with 16 and 32 modes, the higher modes are corrected significantly (which may also indicate a lack of numerical accuracy) and the modified ROMs lose the robustness of the underlying Galerkin models.

#### Comparison

A comparison of ROMs derived using all four approaches (pure Galerkin projection, fully optimized, calibrated, and modified viscous terms) for the controlled LPT flow is shown in Fig. 11. The amplitude $A$ was computed as $A = \sqrt{a_1^2 + a_2^2}$ and the phase was computed as $\varphi = \text{atan}(a_2/a_1)$. Care was taken to assure that the phase was increasing monotonously in time. Shown in Fig. 11 is the difference between the amplitude and phase of the ROM predictions and the reference data, $\Delta A$ and $\Delta\varphi$, respectively. Results obtained with the fully optimized models fall right on top of the results obtained with the calibrated models. No results are shown for the fully optimized model with eight modes, which was numerically unstable. The pure Galerkin models were found to perform worse when more modes were included, displaying significant amplitude and phase errors. The opposite effect should have been expected, and the trend observed can likely be attributed to the structural instability of these models [7]. Modification of the viscous terms according to Eq. (46) improves the model accuracy, however, not in a fully satisfactory manner. Both amplitude and phase error are reduced to almost zero when the model coefficients are fully optimized or calibrated. The fully optimized models were, however, found to be extremely unstable. A stable, fully optimized model with eight modes could not be obtained. From the results presented in this section, it was concluded that the fully optimized models were the most accurate but the least robust. A good balance between robustness and accuracy was achieved when the calibration procedure by Couplet et al. [15] was employed. In the remaining part of the paper, ROMs with control input will be considered.

#### Inclusion of Forcing Terms

The model coefficients that describe how the control input affects the dynamics of the ROM can be obtained by the following procedure:

1) The flow is controlled with a harmonic actuation (e.g., $F^+ = 1/0.2 = 5$ for the LPT case) in an open-loop fashion. A ROM based on a POD basis is then generated for this operating point.

2) The actuation is changed slightly (for example, $F^+ = 1/0.19 = 5.263$ or $F^+ = 1/0.15 = 6.667$) and the time coefficients are

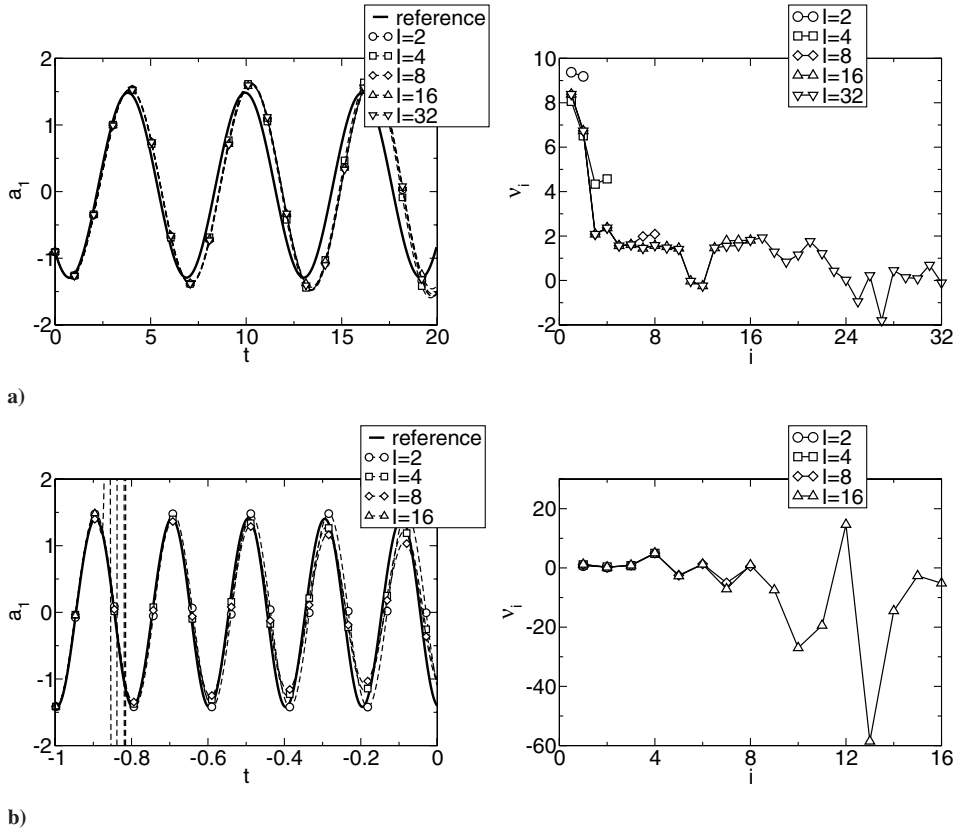


**Fig. 10 Quadratic ROMs with modified viscous terms; mode 1 time coefficient (left) and correction of viscous terms (right): a) circular cylinder flow and b) controlled LPT flow.**

obtained by projection on the POD basis from item 1. If the new operating point is close to the old one, the dynamics of the flow are still captured accurately by the ROM from item 1. If the new operating point is too far from the old one, the set of basis functions is inappropriate and the ROM will not be able to capture the dynamics accurately. The missing actuation coefficients are then determined by the error-minimization technique [minimizing Eq. (21)] with the time coefficients obtained from the projection, the ROM coefficients from item 1, and the known control input.

The accuracy of the ROM with forcing terms and control input is determined by predicting the dynamics of the controlled flow over the time period from item 2 and comparing with the time coefficients obtained from the projection.

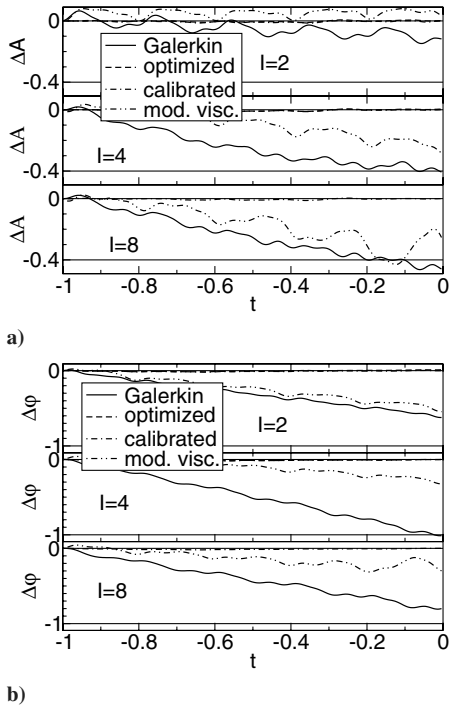


**Fig. 11 Differences between predicted and reference data modes 1 and 2 for ROMs of controlled LPT flow: a) amplitude $\Delta A$ and b) phase $\Delta\varphi$ error.**

*Test Case 1: Change in Actuation Frequency from* $1/0.20$ *to* $1/0.19$

The LPT flow is controlled with $F^+ = 1/0.20 = 5$ for $-1 < t \leq 0$ and $F^+ = 1/0.19 = 5.263$ for $0 < t \leq 5$ (Fig. 12a). Because the POD base computed for the controlled flow with $F^+ = 5$ is used for describing the controlled flow with $F^+ = 1/0.19$, only the change or difference in actuation (curve for $a_{-1}$ in Fig. 12a) enters the ROM. The error-minimization technique is used to compute only the ROM coefficients associated with the control input. The time coefficients for $t > 0$ are computed by projecting the corresponding flow data on the POD basis computed for $-1 < t \leq 0$, $a_i^n = 1/\lambda_i(\mathbf{v}^n, \mathbf{q}_i)_\Omega$. Because the POD basis was computed for $-1 < t < 0$, it well describes the flow controlled with $F^+ = 1/0.20$. Most of the energy is in the lower POD modes, with a pronounced energy dropoff toward the higher modes (Fig. 12b). The mode energy content of the controlled flow for $t > 0$ was computed as $e_i = 1/2\langle\tilde{a}_i\tilde{a}_i\rangle$, where $\tilde{a}_i = \sqrt{\lambda_i}a_i$. As the flow control with $F^+ = 1/0.19$ becomes effective, the flow dynamics shift away from the first operating point, $F^+ = 1/0.20$, for which the POD basis was created. Because the actuation frequency $F^+$ was only slightly modified, modes 1 and 2 still describe the most energetic coherent structures quite well and, therefore, still contain considerably more energy than the remaining modes. However, the energy content of the lower POD modes is reduced overall. The missing energy is accounted for by larger amounts of energy in the higher modes and also, in general, by a larger error of the reconstruction (meaning that the model captures less of the kinetic energy of the flow). The error of the flow reconstruction was computed over all grid points $M$ of the computational domain:

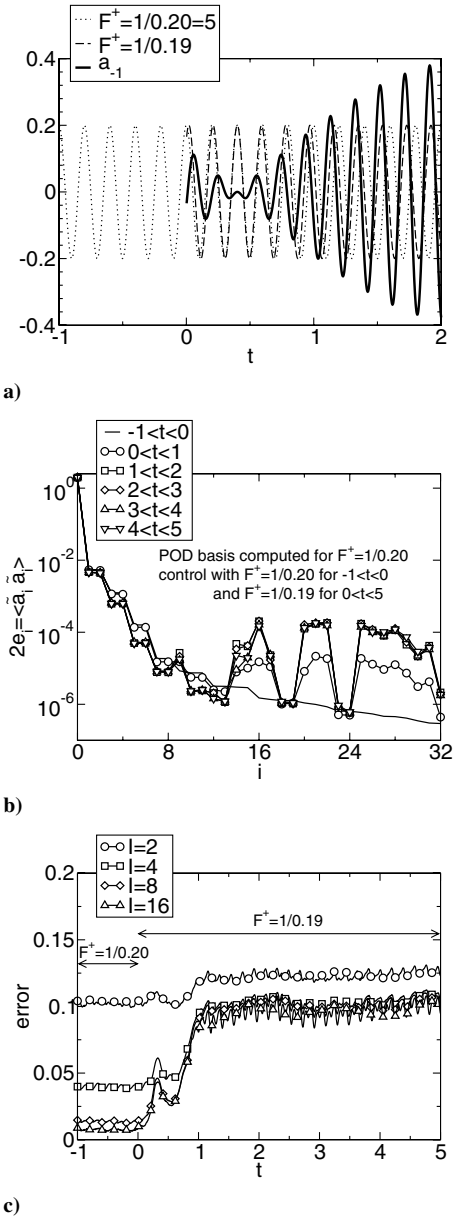


**Fig. 12 ROMs with control input; small change in actuation frequency: a) control input $a_{-1}$ (actuation mode) for controlled LPT flow, b) kinetic energy $e_i$ in respective POD modes, and c) error of flow reconstruction.**

$$\text{error}\,(t) = \sqrt{\frac{1}{M}\sum_{M}\left(\mathbf{v}(t) - \sum_{i=0}^{I} a_i(t)\mathbf{q}_i\right)^2} \tag{50}$$

where $\mathbf{v}(t)$ represents the original flow data and $\sum a_i(t)\mathbf{q}_i$ corresponds to the reconstructed flow data. For $0 < t \leq 1$, the error can be reduced by including more modes (Fig. 12c). This is not the case for $t > 1$, in which a considerable dropoff in mode energy can be observed only up to $i = 4$. The error is not reduced in a significant manner when more than four modes are included.

The control input $a_{-1}$ (flow controlled with $F^+ = 1/0.19$ for $0 < t \leq 5$) enters the ROM derived for $-1 < t \leq 0$ (flow controlled with $F^+ = 1/0.20$) through the forcing coefficients $f_{ij}$, which were computed such that the model prediction error was minimized over the time interval $2 < t \leq 5$. Models were sought that describe the new time-periodic state. The transient phase in which the flow adjusts to the new control for $0 < t \leq 2$ was deliberately excluded because it was shown that such models require a higher model complexity [7]. Results are shown in Fig. 13. Robust models with up to eight modes were obtained when the coefficients of the original ROM were taken

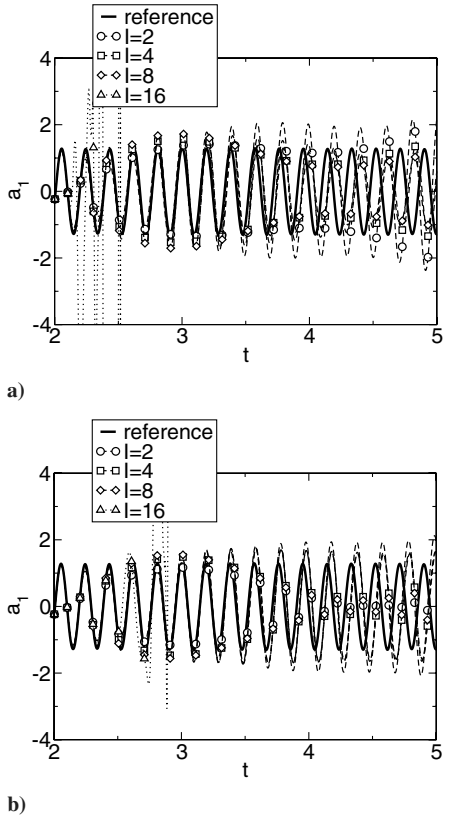


**Fig. 13 Quadratic ROMs with control input; control changes from $F^+ = 1/0.20 = 5$ for $-1 < t \leq 0$ to $F^+ = 1/0.19$ for $0 < t \leq 5$: a) ROM coefficients from Galerkin projection and b) ROM coefficients calibrated with $\alpha = 0.05$.**

from a Galerkin projection. Models with four and eight modes track the reference data well for $t < 2.5$, but underpredict the oscillation amplitude for $t > 3.5$ (Fig. 13a). All models exhibit a growing phase error for $t > 3.5$ that approaches 90 deg for $t = 5$. Models of the controlled flow based on a ROM with fully optimized coefficients turn out to be not very robust (not shown). Models of the controlled flow in which the coefficients of the underlying ROMs were calibrated perform better, both in terms of accuracy and robustness (Fig. 13b). Models with four and eight modes display very good behavior over a time horizon of approximately three shedding cycles and may be considered for controller development.

*Test Case 2: Change in Actuation Frequency from* $1/0.20$ *to* $1/0.15$

For a larger change in actuation frequency from $F^+ = 1/0.20 = 5$ for $-1 < t \leq 0$ to $F^+ = 1/0.15 = 6.667$ for $0 < t \leq 5$, the modes 1 and 2 amplitudes almost vanish for $t > 0$, indicating that these modes are no longer dominant (Fig. 14b). More energy is contained in the higher modes than in the lower modes. This leads to the conclusion that a model based on the lower modes will contain only a small portion of the kinetic energy of the flow and cannot accurately capture the flow dynamics. The error of the reconstructed solution (Fig. 14c) is twice as large as in the previous case and (for $t > 1$) does not decrease when more modes are included. In short, the operating point has moved too far away from the point for which the underlying POD basis was generated. Not surprisingly, ROMs with calibrated forcing terms $f_{ij}$ do not work at all (Fig. 15) and are not appropriate for controller development.

### Composite ROM of LPT Flow Controlled with $F^+ = 1/0.20$ and $F^+ = 1/0.15$

More general ROMs that describe more than one operating point can be constructed by combining POD modes from different operating points [7,8]. Here, a composite model is constructed that contains modes from two operating points, $F^+ = 1/0.20$ (operating

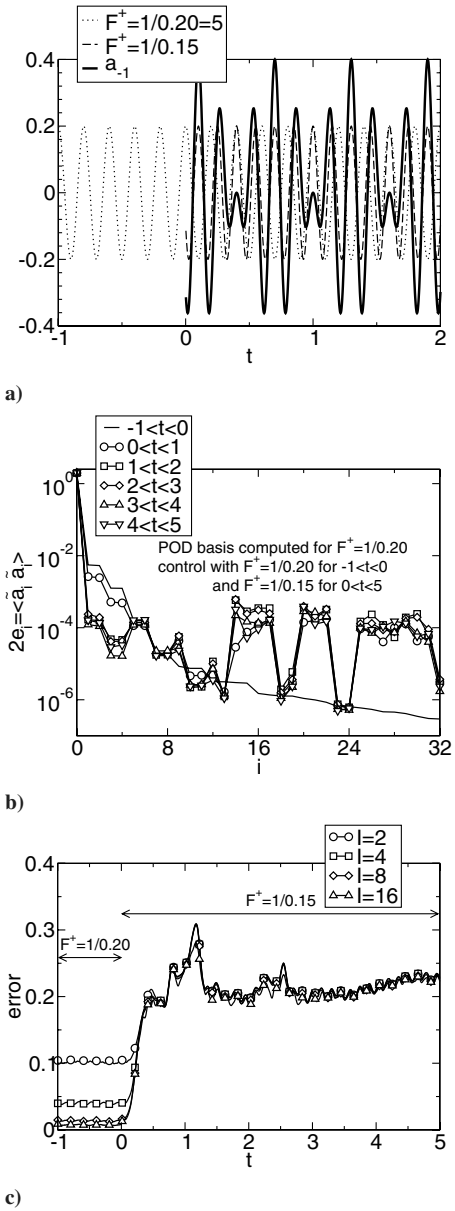


**Fig. 14 ROMs with control input; large change in actuation frequency: a) control input $a_{-1}$ (actuation mode) for controlled LPT flow, b) kinetic energy $e_i$ in respective POD modes, and c) error of flow reconstruction.**

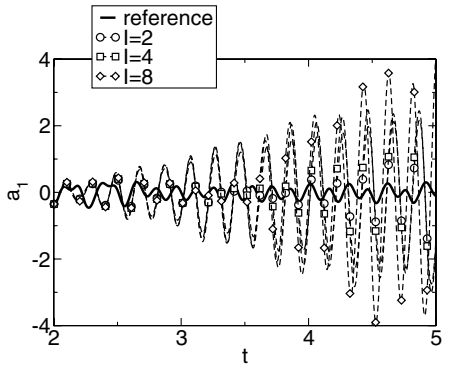


**Fig. 15 Quadratic ROMs with control input; control changes from $F^+ = 1/0.20 = 5$ for $-1 < t \leq 0$ to $F^+ = 1/0.15$ for $0 < t \leq 5$; and ROM coefficients calibrated with $\alpha = 0.05$.**

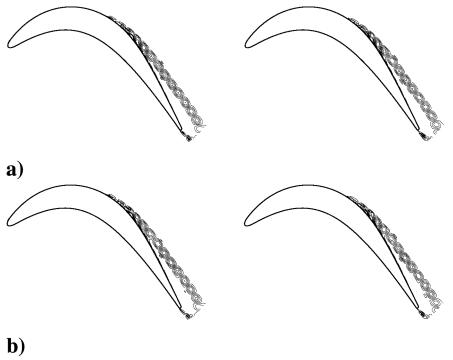


**Fig. 16 Isocontours of vorticity for a) first two modes from POD of flow controlled with $F^+ = 1/0.15$ and b) the same modes after orthogonalization.**

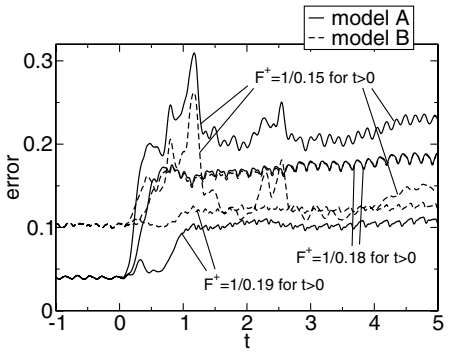


**Fig. 17 Error of flow reconstruction for various operating point 3 forcing frequencies $F^+$.**

point 1) and $F^+ = 1/0.15$ (operating point 2). A POD of the flow controlled with $F^+ = 1/0.20$ ($-1 < t \leq 0$) provides eigenfunctions for operating point 1, whereas a POD of the flow controlled with $F^+ = 1/0.15$ ($4 < t \leq 5$) provides eigenfunctions for operating point 2. The time average of the flow controlled with $F^+ = 1/0.20$ for $-1 < t \leq 0$ is taken as mode 0. The resulting composite modal basis is orthogonalized using the Gram–Schmidt procedure (Fig. 16). This model basis is henceforth referred to as model B. A so-called shift mode [7,8] can be added that describes how the change in control affects the mean flow. Inclusion of the shift mode does not, however, account for the "deformation" of the other POD modes and did not, for the cases studied here, considerably improve model accuracy (not shown).

A model derived for two operating points may describe in-between operating points more accurately than a model derived for only one operating point. To test this hypothesis, a modal basis with four modes taken from a POD of the flow controlled with $F^+ = 1/0.20$ (henceforth referred to as model A) was constructed and compared with model B. The quality of the two modal bases was assessed by projecting flow data from simulations in which the flow was controlled with $F^+ = 1/0.15$, $F^+ = 1/0.18$, and $F^+ = 1/0.19$ (this operating point is henceforth referred to as operating point 3) on the two different modal bases and by computing the error of the flow reconstruction [Eq. (50)]. Results are shown in Fig. 17. As expected, model A is more accurate than model B when operating point 3 is closer to operating point 1, and model B is more accurate than model A when operating point 3 is closer to operating point 2. Results for an operating point 3 identical to operating point 2 ($F^+ = 1/0.15$) are shown in Fig. 18. Model A describes operating point 1 better than model B, but fails to describe operating point 2. For model B, the error reaches its maximum value during the transition period $0 < t \leq 1$, indicating that neither of the two pairs of modes describes the dynamics of the transient regime very well. During the transition period $0 < t \leq 1$, the modes 1 and 2 amplitudes decay, whereas the modes 3 and 4 amplitudes grow. Not surprisingly, the composite model (model B) captures more of the flow dynamics (lower error) for $t > 3$. The composite model can be calibrated simultaneously for operating points 1 and 2 (time intervals $-1 < t \leq 0$ and $4 < t \leq 5$)

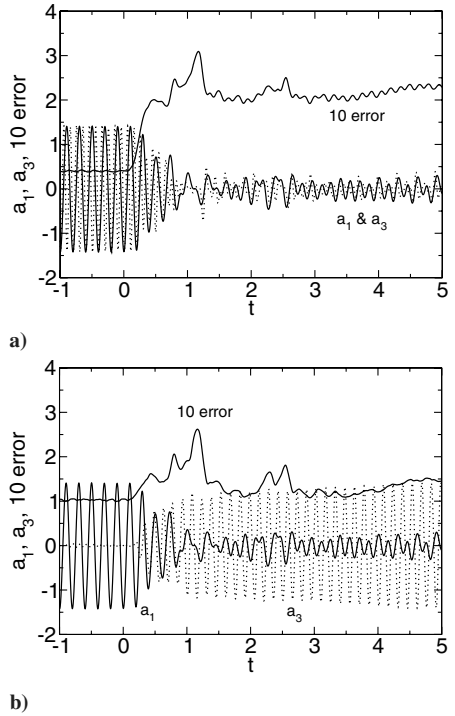


**Fig. 18 Time coefficients $a_1$ and $a_3$ obtained from projection of flow data on a) model A and b) model B eigenfunctions and error (10 times the error) of flow reconstruction.**

by computing the time averages in the calibration procedure as

$$\langle \ldots \rangle = \int_{-1}^{0} \ldots \, \mathrm{d}t + \int_{4}^{5} \ldots \, \mathrm{d}t \tag{51}$$

The resulting calibrated composite model with four modes describes both operating points very well (Fig. 19b). For the uncalibrated Galerkin model, the flow prediction for operating point 2 deviates from the reference (Fig. 19a). The ultimate goal, of course, is to use the derived composite models for control purposes. Preliminary results with models A and B and control input [31] show some potential and also suggest that continued model development and improvement are required before this class of ROMs becomes viable for control applications.

## Conclusions

Various reduced-order models for predicting a time-dependent circular cylinder flow and an uncontrolled and open-loop controlled low-pressure turbine flow were designed and studied. ROMs were obtained by a Galerkin projection of the governing equations (the incompressible Navier–Stokes equations) on a proper orthogonal decomposition modal basis. These ROMs were found to be relatively inaccurate but robust when compared with ROMs that were fully optimized to match the reference data with minimal error. The inaccuracies were attributed to the simplifying assumptions made (assumption of incompressible flow for model derivation, although simulation was based on compressible equations; neglect of boundary terms arising from the Galerkin projection), numerical inaccuracies (the flow solver was finite volume and employed different discretization than the Galerkin projection), and the model truncation (higher modes dissipate energy; model truncation leads to energy accumulation in the lower modes). Fully optimized models were found to be very accurate but lack robustness. Small disturbances can result in rapid and catastrophic failure of the model. As a mixture of the first two approaches, the Galerkin models were calibrated to better track the POD time coefficients [15]. The resulting models were shown to be both accurate and robust. Other ideas with the goal of modifying the Galerkin model coefficients such that the change in modal energy content over a certain time interval was minimized or equal to the reference data did not result in significantly more accurate and robust models. In general, models that are built from fewer modes appeared to be more robust but less accurate than models that are built from a larger number of modes. Also, ROMs were found to perform noticeably better for organized,

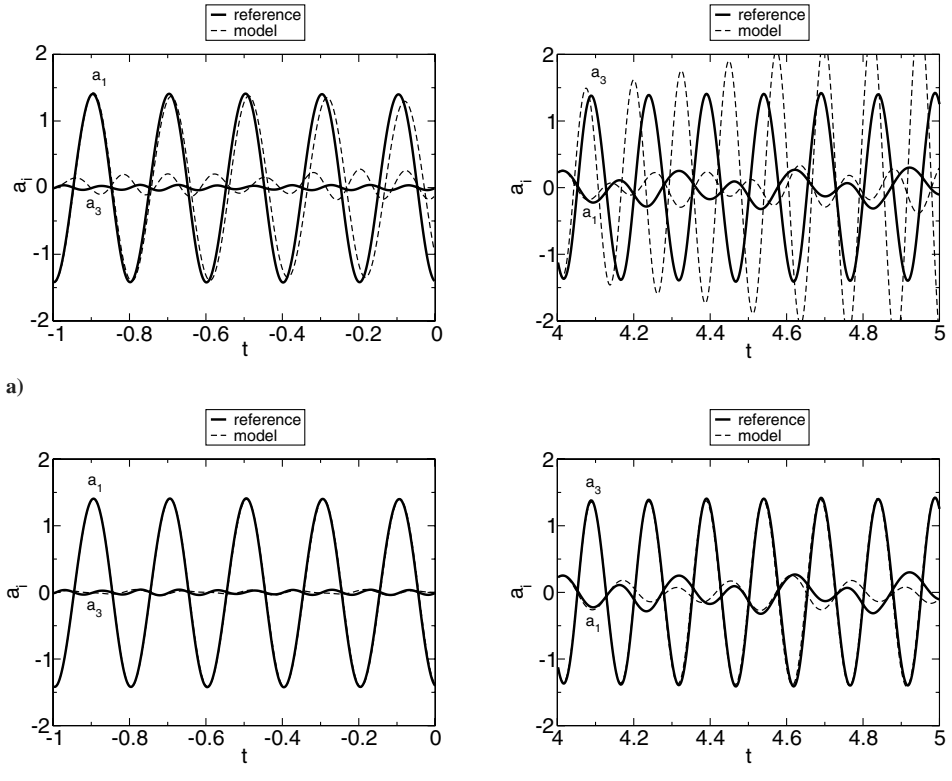


**Fig. 19 Comparison of model prediction with reference data for operating point 1 (left) and operating point 2 (right) for a) uncalibrated and b) calibrated composite model.**

time-periodic flows (the LPT flow was made time-periodic by harmonic actuation) than for chaotic, less organized flows.

For ROMs to be of use for control purposes, they must be capable of describing the effect of the control/actuation on the flow dynamics. For time-dependent actuation (especially, for complicated geometries and/or actuators), more than one additional mode may be needed to accurately describe the interaction of the control with the flow. In this paper, only one control mode was considered. However, the procedure presented here can easily be extended to allow for more than one control input. The forcing coefficients (the coefficients that describe how the forcing or actuation enters the model) were obtained by minimizing the difference between the ROM prediction of the flow dynamics and the actual observed flow dynamics. This optimization was performed for a time interval in which the flow was already completely locked in to the control. Thus, the transient was deliberately excluded in this optimization. The reasoning behind this approach was to find a model for two time-periodic operating points and to then develop a controller that would not exploit the transients of the system and only gradually change the dynamics of the system. The resulting models with control input were shown to work well only close to the design operating point. Composite models that describe more than one operating point can be constructed by combining POD modes from different operating points (flow controlled with different frequencies). Results obtained with a composite model that was designed for two operating points demonstrate the advantage of composite models, namely, their greater versatility.

In summary, calibrated ROMs were shown to very accurately describe the dynamics of time-dependent flows even when simplifying assumptions were made during the derivation of the Galerkin models on which the calibrated models were based. ROMs with control input, in which the forcing coefficients were obtained from an optimization procedure aimed at minimizing the difference between the model prediction and the actual flow behavior, were shown to perform reasonably well in the vicinity of the design operating point of the underlying model without control. It remains to be shown that the accuracy and robustness of the resulting ROMs is sufficient for them to become practical for controller design and flow control applications.

## Acknowledgments

This work was funded by the Deutsche Forschungsgemeinschaft (DFG) under grant number GR 2117/1-1 and by the U.S. Air Force Office of Scientific Research (AFOSR) under grant number F9550-05-1-0166.

## References

[1] Collis, S. S., Joslin, R. D., Seifert, A., and Theofilis, V., "Issues in Active Flow Control: Theory, Control, Simulation, and Experiment," *Progress in Aerospace Sciences*, Vol. 40, Nos. 4–5, 2004, pp. 237–289.

[2] Joslin, R. D., Gunzburger, M. D., Nicolaides, R. A., Erlebacher, G., and Hussaini, M. Y., "A Self-Contained, Automated Methodology for Optimal Flow Control Validated for Transition Delay," *AIAA Journal*, Vol. 35, No. 5, 1997, pp. 816–824.

[3] Bewley, T. R., Moin, P., and Temam, R., "DNS-Based Predictive Control of Turbulence: An Optimal Benchmark for Feedback Algorithms," *Journal of Fluid Mechanics*, Vol. 447, 2001, pp. 179–225.

[4] Glauser, M.N., Higuchi. H., Ausseur, J., Pinier, J., and Carlson. H., "Feedback Control of Separated Flows," AIAA Paper 2004-2521, 2004

[5] Pastoor, M., King, R., Noack, B.R., Dillmann, A., and Tadmor, G., "Model-Based Coherent-Structure Control of Turbulent Shear Flows Using Low-Dimensional Vortex Models," AIAA Paper 2003-4261, June 2003.

[6] Gerhard, J., Pastoor, M., King, R., Noack, B. R., Dillmann, A., Morzyński, M., and Tadmor, G., "Model-Based Control of Vortex Shedding Using Low-Dimensional Galerkin Models," AIAA Paper 2003-4262, June 2003.

[7] Noack, B. R., Afanasiev, M. M., Tadmor, G., and Thiele, F., "A Hierarchy of Low-Dimensional Models for the Transient and Post-Transient Cylinder Wake," *Journal of Fluid Mechanics*, Vol. 497, 2003, pp. 335–363.

[8] Noack, B. R., Tadmor, G., and Morzyński, M., "Low-Dimensional Models for Feedback Flow Control, Part 1: Empirical Galerkin Models," AIAA Paper 2004-2408, 2004.

[9] Tadmor, G., Noack, B. R., Morzyński, M., and Siegel, S., "Low-Dimensional Models For Feedback Flow Control, Part 2: Control Design and Dynamic Estimation," AIAA Paper 2004-2409, 2004.

[10] Morzyński, M., Afanasiev, K., and Thiele, F., "Solution of the Eigenvalue Problems Resulting from Global Nonparallel Flow Stability Analysis," *Computer Methods in Applied Mechanics and Engineering*, Vol. 169, Nos. 1–2, 1999, pp. 161–176.

[11] Abdessemed, N., Sherwin, S. J., and Theofilis, V., "On Unstable 2D Basic States in Low Pressure Turbine Flows at Moderate Reynolds Numbers," AIAA Paper 2004-2541, 2004.

[12] Gross, A., and Fasel, H. F., "Simulation of Active Flow Control for a Low Pressure Turbine Blade Cascade," AIAA Paper 2005-0869, Jan. 2005.

[13] Aubry, N., Holmes, P., Lumley, J. L., and Stone, E., "The Dynamics of Coherent Structures in the Wall Region of a Turbulent Boundary Layer," *Journal of Fluid Mechanics*, Vol. 192, 1988, pp. 115–173.

[14] Ukeiley, L., Cordier, L., Manceau, R., Delville, J., Glauser, M., and Bonnet, J. P., "Examination of Large-Scale Structures in a Turbulent Plane Mixing Layer, Part 2: Dynamical Systems Model," *Journal of Fluid Mechanics*, Vol. 441, 2001, pp. 67–108.

[15] Couplet, M., Basdevant, C., and Sagaut, P., "Calibrated Reduced-Order Pod-Galerkin System for Fluid Flow Modelling," *Journal of Computational Physics*, Vol. 207, No. 1, 2005, pp. 192–220.

[16] Sirisup, S., and Karniadakis, G. E., "A Spectral Viscosity Method for Correcting the Long-Term Behavior of Pod Modes," *Journal of Computational Physics*, Vol. 194, No. 1, 2004, pp. 92–116.

[17] Rempfer, D., "On Low-Dimensional Galerkin Models for Fluid Flow," *Theoretical and Computational Fluid Dynamics*, Vol. 14, No. 2, 2000, pp. 75–88

[18] Gross, A., and Fasel, H. F., "Numerical Investigation of Low-Pressure Turbine Blade Separation Control," *AIAA Journal*, Vol. 43, No. 12, 2005, pp. 2514–2525.

[19] Lumley, J. L., "The Structure of Inhomogeneous Turbulent Flows," *Atmospheric Turbulence and Radio Wave Propagation*, edited by A. M. Yaglom and V. I. Tatarsky, Nauka, Moscow, 1967, pp. 166–178.

[20] Sirovich, L., "Turbulence and the Dynamics of Coherent Structures," *Quarterly of Applied Mathematics*, Vol. 45, No. 3, 1987, pp. 561–590

[21] Noack, B. R., Papas, P., and Monkewitz, P. A., "The Need for a Pressure-Term Representation in Empirical Galerkin Models of Incompressible Shear Flows," *Journal of Fluid Mechanics*, Vol. 523, 2005, pp. 339–365.

[22] Gillies, E. A., "Low-Dimensional Control of the Circular Cylinder Wake," *Journal of Fluid Mechanics*, Vol. 371, 1998, pp. 157–178.

[23] Ausseur, J. M., and Pinier, J. T., "Towards Closed-Loop Feedback Control of the Flow over NACA-4412 Airfoil," AIAA Paper 2005-0343, Jan. 2005.

[24] Iollo, A., Lanteri, S., and Désidéri, J.-A., "Stability Properties of POD-Galerkin Approximations for the Compressible Navier–Stokes Equations," *Theoretical and Computational Fluid Dynamics*, Vol. 13, No. 6, 2000, pp. 377–396.

[25] Rowley, C. W., Colonius, T., and Murray, R. M., "Model Reduction for Compressible Flows Using Pod and Galerkin Projection," *Physica D*, Vol. 189, Nos. 1–2, 2004, pp. 115–129.

[26] Prudhomme, S., and Le Letty, L., "A Low-Order Model-Following Strategy for Active Flow Control," *IUTAM Symposium on Mechanics of Passive and Active*, edited by G. E. A. Meier and P. R. Viswanath, Kluwer Academic, Dordrecht, The Netherlands, 1999, pp. 355–366

[27] Deane, A. E., Kevrekidis, I. G., Karniadakis, G. E., and Orzag, S. A., "Low-Dimensional Models for Complex Geometry Flows: Application to Grooved Channels and Circular Cylinders," *Physics of Fluids A*, Vol. 3, No. 10, 1991, pp. 2337–2354.

[28] Sondergaard, R., Bons, J. P., and Rivir, R. B., "Control of Low-Pressure Turbine Separation Using Vortex Generator Jets," *Journal of Propulsion and Power*, Vol. 18, No. 4, 2002, pp. 889–895.

[29] Schlichting, H., and Gersten, K., *Boundary Layer Theory*, Springer, New York, 2004.

[30] Rempfer, D., "Low-Dimensional Modeling and Numerical Simulation of Transition in Simple Shear Flows," *Annual Review of Fluid Mechanics*, Vol. 35, 2003, pp. 229–265.

[31] Gross, A., and Fasel, H. F., "Reduced Order Models for Closed-Loop Control of Time-Dependent Flows," AIAA Paper 2006-1403, Jan. 2006.

X. Zhong
*Associate Editor*